Electronic Supplementary Information for Dalton Transactions

Electronic Supplementary Information

Synthesis and characterisation of low valent Mn-complexes as models for Mn-catalases

Gustav Berggren, Ping Huang, Lars Eriksson, Stenbjörn Styring, Magnus F. Anderlund, Anders Thapper*

Table S1 Selected bond lengths (Å) for **1.**

Bond	**x = 1, y = 3**	**x = 2, y = 1**	**x = 3, y = 2**	**Average (x = 1–3)**
Mnx–Ox02	2.104(9)	2.109(8)	2.136(9)	2.12(2)
Mnx–Ox01	2.151(8)	2.119(9)	2.138(10)	2.14(2)
Mnx–Nx11	2.350(10)	2.356(11)	2.384(11)	2.36(2)
Mnx–Nx12	2.351(8)	2.427(10)	2.284(10)	2.35(7)
Mnx–Nx21	2.322(10)	2.224(12)	2.221(11)	2.26(6)
Mnx–Nx22	2.226(9)	2.249(5)	2.222(10)	2.23(2)
Mnx–Oy01	3.222(10)	3.005(8)	3.324(9)	3.2(2)

Table S2 Manganese–manganese distances (Å) in **1**.

Mn1–Mn2	5.062(3)
Mn1–Mn3	5.309(3)
Mn2–Mn3	5.402(3)
Mn1–Mn1[a]	10.525(3)
Mn1–Mn2[a]	10.656(2)
Mn1–Mn3[a]	11.864(3)
Mn2–Mn2[a]	11.788(3)
Mn2–Mn3[a]	10.561(3)
Mn3–Mn3[a]	10.728(3)
<135>–<246> [b]	11.0(6)

[a] Symmetry related position: 1.5-x, 0.5-y, z

[a] Distance (<135>–<246>) is the distance between the centre of gravity points of the metal ions of the two trimeric 12-membered metallamacrocycles present in the structure of **1**.

Table S3 Selected bond angles (°) in **1**.

Bond angle	x=1	x=2	x=3	Average
Ox01-Mnx-Ox02	97.9(4)	103.0(3)	95.0(4)	98(4)
Ox01-Mnx-Nx11	100.6(3)	86.8(4)	104.6(4)	97(9)
Ox01-Mnx-Nx12	73.7(3)	74.9(3)	74.9(3)	74.5(7)
Ox01-Mnx-Nx21	168.2(4)	160.1(4)	168.1(4)	166(5)
Ox01-Mnx-Nx22	82.5(3)	93.2(3)	89.4(4)	88(5)
Ox02-Mnx-Nx11	154.5(3)	159.6(4)	157.2(4)	157(3)
Ox02-Mnx-Nx12	91.2(3)	88.5(3)	96.8(3)	92(4)
Ox02-Mnx-Nx21	86.7(4)	88.5(4)	86.1(3)	87.1(12)
Ox02-Mnx-Nx22	126.5(4)	123.7(3)	118.6(4)	123(4)
Nx11-Mnx-Nx12	77.4(3)	76.7(4)	77.5(4)	76.9(4)
Nx11-Mnx-Nx21	72.0(3)	77.5(5)	72.3(4)	74(3)
Nx11-Mnx-Nx22	73.6(4)	72.7(3)	73.9(4)	73.4(6)
Nx12-Mnx-Nx21	95.4(3)	89.4(4)	93.2(4)	93(3)
Nx12-Mnx-Nx22	138.0(4)	147.7(3)	142.6(4)	143(5)
Nx21-Mnx-Nx22	103.6(4)	93.7(3)	100.5(4)	99(5)

Table S4 Selected bond lengths (Å) in **2**.

Mn1–N11	2.273(3)	Mn2–N21	2.253(3)
Mn1–N12	2.239(3)	Mn2–N22	2.284(3)
Mn1–N13	2.352(3)	Mn2–N23	2.368(3)
Mn1–N14	2.309(3)	Mn2–N24	2.300(3)
Mn1–O3	2.057(2)	Mn2–O1	2.048(2)
Mn1–Cl1	2.5551(10)	Mn2–Cl1	2.5857(10)
Mn1–Mn2	4.073(1)		

Table S5 Selected bond angles (°) in **2**.

O3-Mn1-N11	95.71(10)	O1-Mn2-N21	96.13(10)
O3-Mn1-N12	89.88(10)	O1-Mn2-N22	89.44(11)
O3-Mn1-N13	160.34(10)	O1-Mn2-N23	159.30(10)
O3-Mn1-N14	116.63(11)	O1-Mn2-N24	115.39(10)
O3-Mn1-Cl1	98.36(7)	O1-Mn2-Cl1	102.76(8)
N11-Mn1-N12	90.43(10)	N21-Mn2-N22	93.70(11)
N11-Mn1-N13	71.97(10)	N21-Mn2-N23	72.64(10)
N11-Mn1-N14	147.55(10)	N21-Mn2-N24	148.47(10)
N11-Mn1-Cl1	89.51(7)	N21-Mn2-Cl1	88.50(8)
N12-Mn1-N13	75.32(10)	N22-Mn2-N23	74.38(11)
N12-Mn1-N14	87.20(11)	N22-Mn2-N24	86.45(11)
N12-Mn1-Cl1	171.72(8)	N22-Mn2-Cl1	167.32(8(
N13-Mn1-N14	76.15(10)	N23-Mn2-N24	77.09(10)
N13-Mn1-Cl1	96.81(7)	N23-Mn2-Cl1	94.44(8)
N14-Mn1-Cl1	88.41(8)	N24-Mn2-Cl1	85.18(8)
Mn1-Cl1-Mn2	104.77(3)		

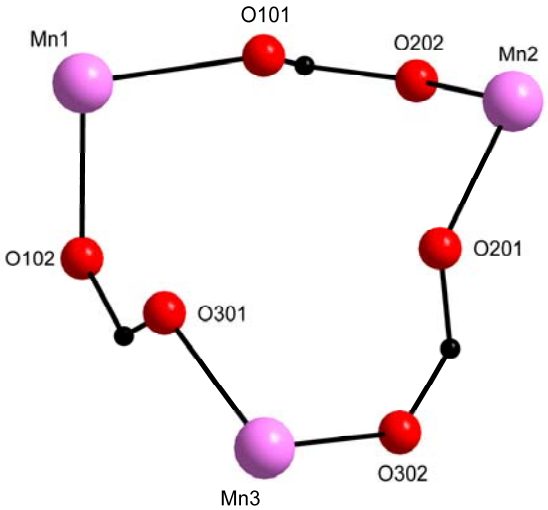

Fig. S1 Perspective view of one of the metallamacrocycles in $[\mathbf{L1}_3Mn_6]^{6+}$, only the atoms constituting the metallamacrocycle are shown for clarity. Colour coding: pink = Mn; red = O; black = C.

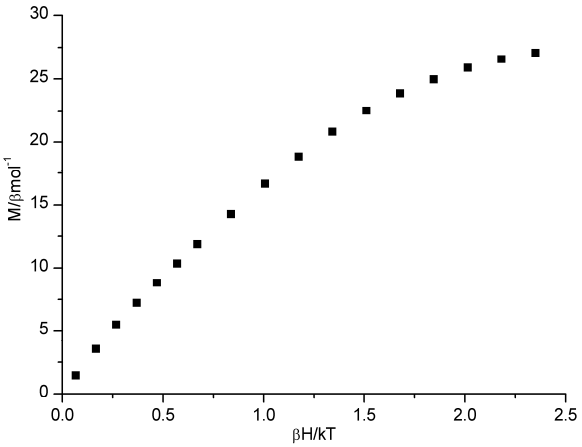

Fig. S2 Magnetization of **1** in response to the applied magnetic field up to 7 T at T = 2 K.

The magnetisation of **1** increased nearly linearly in response to the increased field strength up to 3 T ($\beta H/kT \approx 1$) where it started to deviate from the linearity and reached a value of 27.07 μ_B at 7 T ($\beta H/kT = 2.35$). The failure of the Brillouin function to fit the experimental data suggests that the increase of magnetisation involved an intrinsic intramolecular spin alignment, probably due to the weak antiferromagnetic interaction and the spin frustration. The magnetisation value of 27.07 μ_B is close to the expected value of 28.95 μ_B with $g = 1.93$ for a system with total spin of $S = 15$.

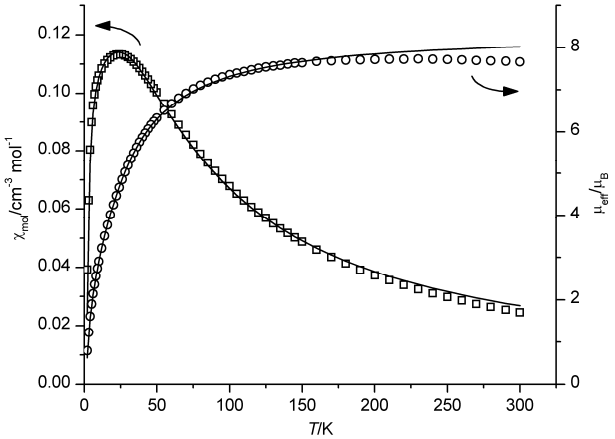

Fig. S3 Molar susceptibility χ_{mol} (□) and effective magnetic moment μ_{eff} (○) of **2** vs. T. Solid lines represent calculated χ_{mol} and μ_{eff} using g = 2.00 and J = –5.67 cm^{-1}.

The molar susceptibility of **2** increased upon cooling until it reached a maximum value at 24 K, followed by a rapid decrease at lower temperature. The best fitting by solving the spin exchange interaction Hamiltonian $H_{ex} = -2JS_1S_2$ using eq. S1 (where x = J/kT)[18] gave g = 2.00 and J = –5.67 cm^{-1}.

$$\chi = \frac{Ng^2\mu_B^2}{kT} \times \frac{2e^{2x} + 10e^{6x} + 28e^{12x} + 60e^{20x} + 110e^{30x}}{1 + 3e^{2x} + 5e^{6x} + 7e^{12x} + 9e^{20x} + 11e^{30x}} \qquad \text{(S1)}$$

The calculated molar susceptibility and effective magnetic moment are shown as solid lines in Fig. S3.

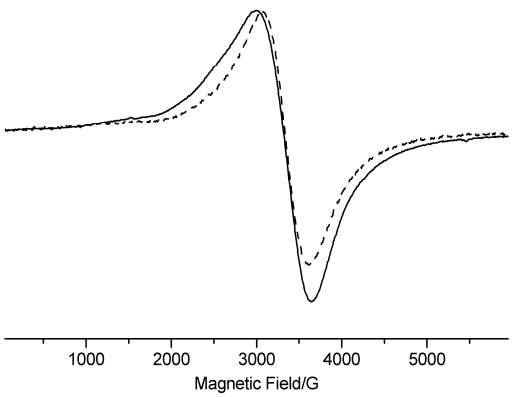

Fig. S4 EPR spectra of **1** in a KBr matrix (dashed line) and in MeCN frozen solution (0.33 mM, solid line). EPR conditions: Microwave frequency 9.27 GHz, microwave power 20 μW; modulation frequency 100 kHz, modulation amplitude 10 G, T = 15 K (KBr matrix), 20 K (in MeCN).

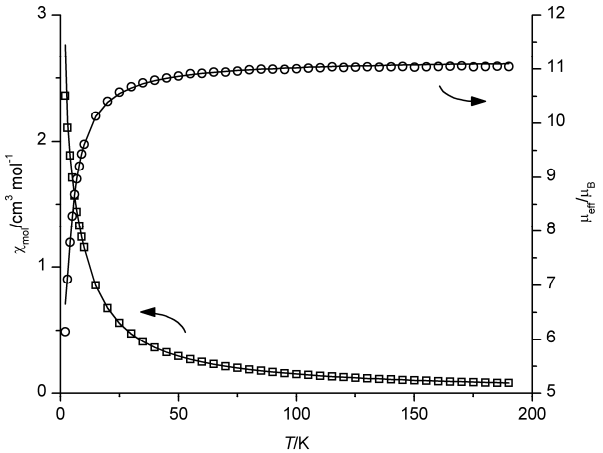

Fig. S5 Molar susceptibility χ_{mol} (□) and effective magnetic moment μ_{eff} (○) of **1** in a (frozen) MeCN solution vs. temperature. Solid lines represent calculated χ_{mol} and μ_{eff} using eqs. 1 and 2 with $g_{eff} = 2.14$ and $J = -1.91$ cm^{-1}.

In Fig. S5 the molar susceptibility, χ_{mol}, and effective magnetic moment, μ_{eff}, of **1** in frozen acetonitrile frozen solution is shown plotted as a function of temperature. The calculation procedure using the same model as for **1** in powder form (see main text) was applied, and resulted in $g_{eff} = 2.14$ and $J = -1.91$ cm^{-1}. These values are comparable with those obtained for **1** as a powder.

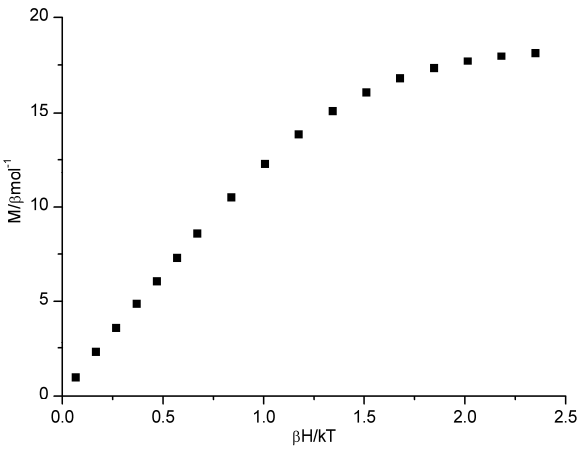

Fig. S6 Magnetization of **1,** in a frozen MeCN solution, in response to the applied magnetic field up to 7 T at T = 2 K.

The magnetisation of **1** in a frozen acetonitrile solution in response to the magnetic field is shown in Fig. S6, the curve is similar to the corresponding curve measured for the powder sample and shows that **1** is spin frustrated also in solution.

The fact that a good fit for χ_{mol} and μ_{eff} was obtained using the same model system as for a powder sample and that the complex still showed spin frustration in a frozen solution justifies the conclusion that **1** retains the hexameric structure in solution. In overall, the solution sample gave χ_{mol} and μ_{eff} values that were lower than those obtained from the powder sample. Similarly, the saturation magnetisation value (~18.2 μ_B) was much lower compared to the 27.1 μ_B found in the powder sample. The discrepancies between the powder sample and the frozen solution sample is attributed to a different degree of spin frustration probably due to minor structural modifications when **1** is dissolved in MeCN.

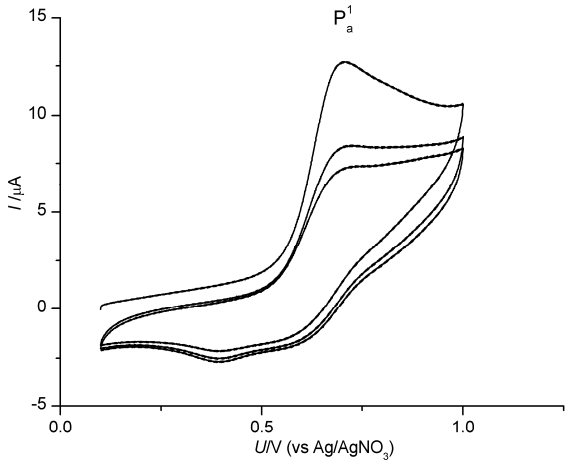

Fig S7 Multiple CV scans for **2** in the range 0.1–1 V, showing a drop in anodic current for each successive scan.

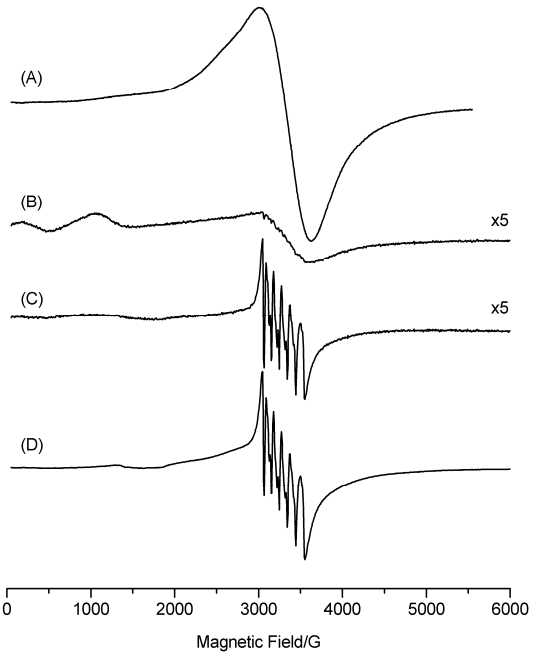

Fig. S8 EPR spectra of **1** (A) before bulk electrolysis and after bulk electrolysis at (B) 0.7 V, (C) 1.05 V, and (D) 1.45 V. Spectra (B) and (C) are magnified 5 times for clarity. EPR parameters: T = 20 K, microwave frequency = 9.28 GHz, microwave power, 0.2 mW, modulation amplitude, 10 G.

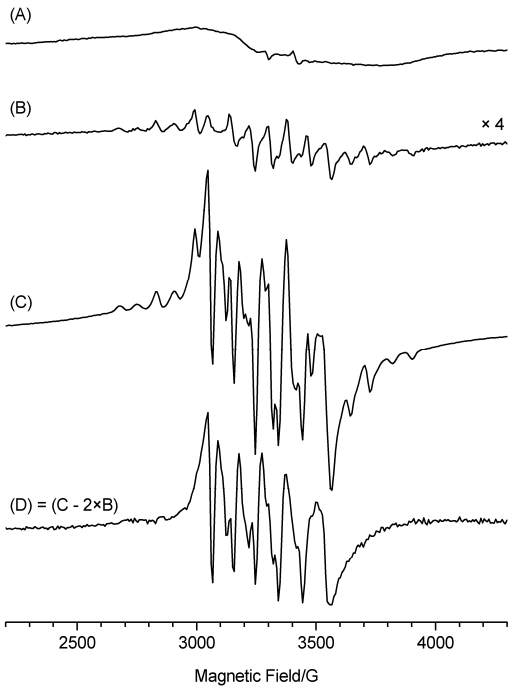

Fig. S9 EPR spectra of complex **2** obtained from bulk electrolysis at 0.95 V. (A) Before bulk electrolysis. (B) EPR spectrum of sample obtained after consumption of 1 electron per Mn, the spectrum is magnified 4 times for clarity. (C) EPR spectrum of sample obtained after consumption of 1.5 electrons per Mn. (D) Difference spectrum (C – 2×B) showing the contribution of a 6-line EPR signal in (C). EPR parameters: T = 5 K, microwave frequency = 9.28 GHz, microwave power, 125 μW, modulation amplitude, 10 G.

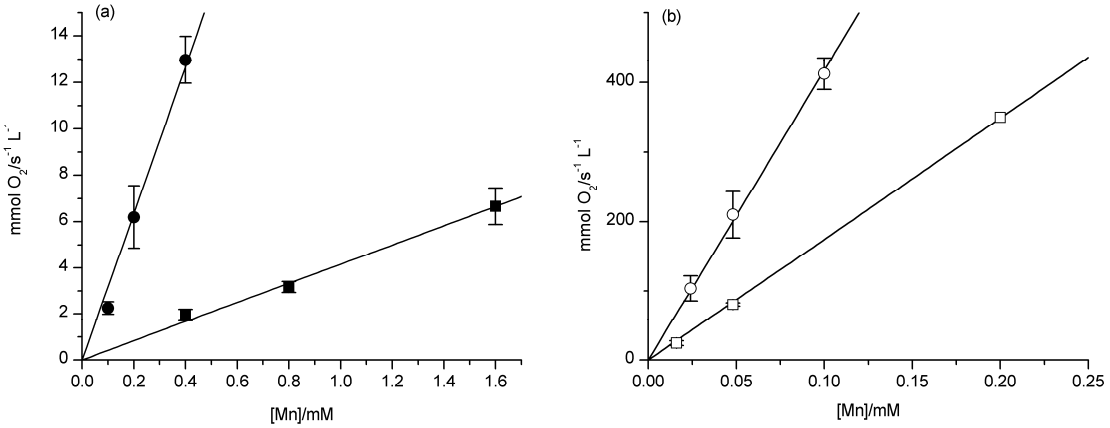

Fig. S10 Rate of oxygen formation vs. catalyst concentration for (a) complex **1** (■) and **3**(●) and (b) complex **2** (□) and **4** (○).

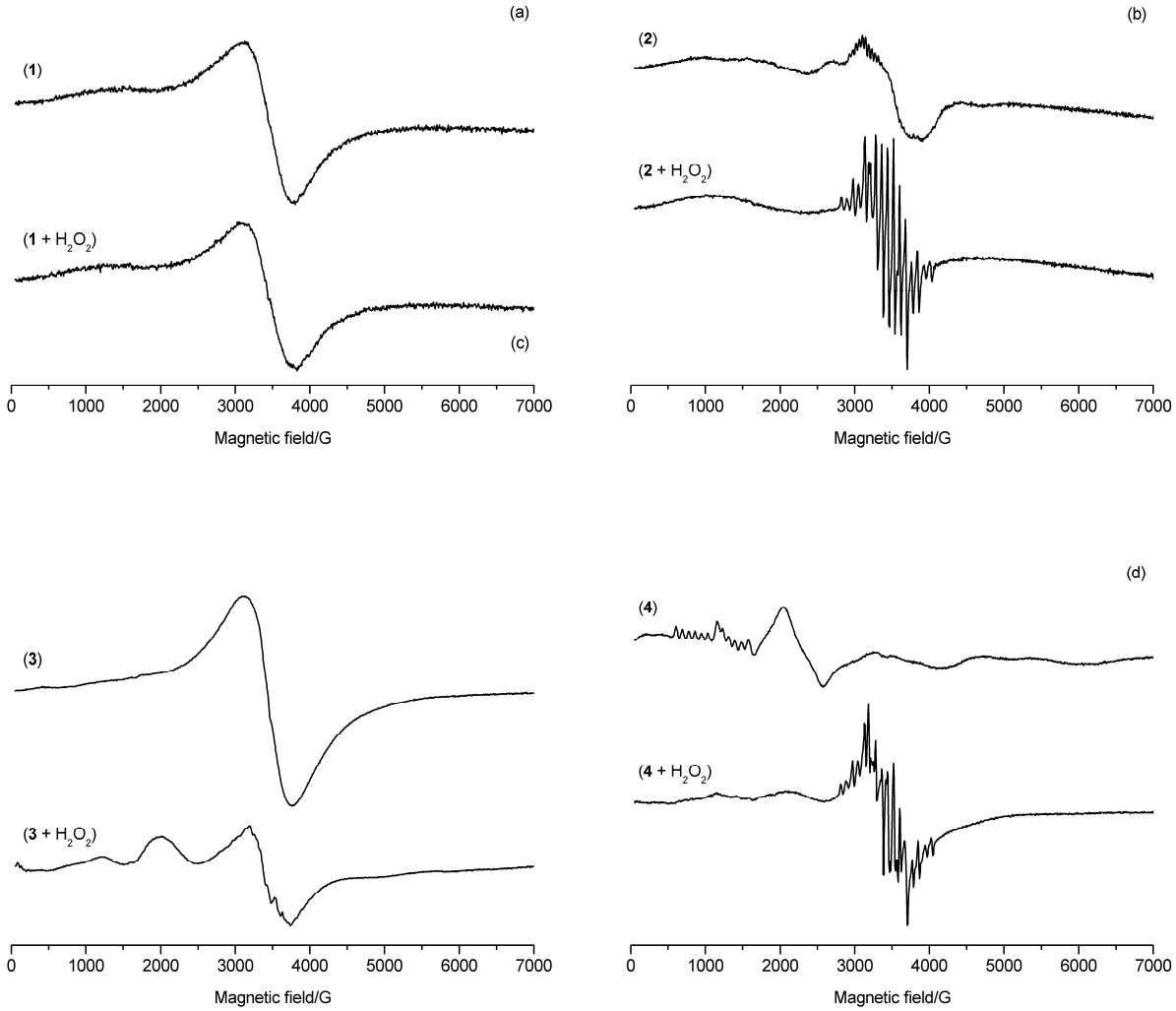

Fig. S11 (a) EPR spectra of **1** before and 3 min after addition of H_2O_2. (b) EPR spectra of **2** before and 15 s after addition of H_2O_2. (c) EPR spectra of **3** before and 90 s after addition of H_2O_2. (d) EPR spectra of **4** before and 15 s after addition of H_2O_2. EPR parameters: T = 5 K (b: T = 20 K), microwave frequency = 9.63 GHz, microwave power, 125 μW (b: power = 2 mW), modulation amplitude, 10 G.